Journal of Sound and Vibration 330 (2011) 1052–1064

Contents lists available at ScienceDirect

Journal of Sound and Vibration

journal homepage: www.elsevier.com/locate/jsvi

Two-degree-of-freedom rotational-pendulum vibration absorbers

Shang-Teh Wu *, Yu-Rong Chen, Se-Si Wang

Department of Mechanical Engineering, National Yunlin University of Science & Technology, Touliu, Yunlin 640, Taiwan

ARTICLE INFO

Article history:
Received 25 May 2010
Received in revised form
24 August 2010
Accepted 25 September 2010
Handling Editor: L.G. Tham
Available online 13 October 2010

ABSTRACT

This paper presents experimental as well as analytic results on a rotational-pendulum vibration absorber. The characteristic frequencies of the absorber can be tuned dynamically by adjusting the rotational speed. The device is coupled to the primary structure through a mechanical spring, thus possessing two natural modes of vibrations in the vertical plane. When the primary structure is excited by a harmonic disturbance of which the frequency matches one of the two natural frequencies, the oscillations will be minimized. Whether the pendulum absorber is operating in a resonant mode can be detected by measuring the phase difference between the motions of the primary structure and the absorber, which provides an efficient way to tune the rotational speed for optimal performance. Experimental results confirm the theoretical developments and also demonstrate the effectiveness of the proposed scheme.

1. Introduction

Pendulum vibration absorbers have been devised in several different configurations for various applications. These include the tuned mass damper (TMD) installed in tall buildings either for mitigation of wind-induced swaying or for seismic protection [1,2], the centrifugal pendulum absorbers for neutralizing torsional disturbances [3,4], and the absorbers mounted on a helicopter's rotor blades for attenuation of aerodynamically induced vibrations [5,6]. Simple pendulums can also be devised as a nonlinear vibration absorber employing *autoparametric resonance*, which is due to a nonlinear coupling between the primary structure and the pendulum subsystem [7–9].

This paper presents experimental as well as analytic results on a rotational-pendulum vibration absorber (Rotational Pendulum Absorber for short, or RPA). The mechanism is a modified design of the pendulum absorber introduced in [10], where an RPA rigidly coupled to the primary structure was analyzed and numerically simulated. The modified RPA is coupled to the primary structure via a mechanical spring, which adds one more degree of freedom to the vibration absorber. As a result, there are two natural frequencies associated with a nominal rotational speed. The two-degree-of-freedom device has the merit of achieving higher characteristic frequency with a relatively low rotational speed, thanks to the second vibration mode. More importantly, the state of the RPA can be detected by measuring the phase angle between the motion of the primary structure and that of the absorber. The phase angle is near 90° when one of the characteristic frequencies matches the excitation frequency. The rotational speed could thus be adjusted according to the magnitude of the detected phase angle. This feature provides an efficient method of tuning the speed for optimal performance. In this paper analytic derivations will be confirmed by both numerical simulation and real-time experiment.

Similar to an active vibration absorber, characteristic frequencies of the RPA can be dynamically tuned over a wide range in order to counter external excitation with either uncertain or time-drifting frequencies. However, unlike the active

* Corresponding author. Tel.: +886 5 5342601x4111; fax: +886 5 5312062.
E-mail address: wust@yuntech.edu.tw (S.-T. Wu).

0022-460X/$ - see front matter © 2010 Elsevier Ltd. All rights reserved.
doi:10.1016/j.jsv.2010.09.028

techniques that rely on an actuator, such as linear electromagnetic actuators [11–13] and electrohydraulic actuators [14], to directly counter the external disturbance, the resisting force of RPA does not come from the actuator but from the inertial force of the revolving pendulum. The scheme may thus be categorized as a "variable stiffness" vibration absorber [15–19]. The actuator (an electric motor) in the RPA serves the purpose of regulating the rotational speed, thereby dynamically setting the stiffness of the pendulum absorber. Once the pendulum reaches the target speed, only minimal power is required to compensate for the rotational frictions. The scheme thus has the flexibility of an active vibration absorber and the energy-efficient merit of a passive device. The device is best suitable for vibrations with a dominant base frequency that may drift over time. Possible applications include suppression of vibrations generated by rotary machines, and interior noise attenuation for a propeller plane [20].

The rest of the paper is organized as follows. Section 2 presents the design and mathematical derivation of the two-degree-of-freedom RPA. Based on the experimental model, numerical analysis about the device's natural frequencies is conducted. Numerical simulations are also conducted to illustrate the performance of the RPA. Section 3 shows how the phase angle between the primary structure and the RPA is related to the rotational speed given an excitation frequency. Experimental results on an RPA prototype are presented in Section 4, where time responses of the primary structure for various operational conditions are recorded and analyzed. Experimental results and theoretical developments are then compared. Section 5 is a brief conclusion of the paper.

2. Rotational-pendulum absorber with a spring coupler

The RPA consists of a pair of symmetric pendulums driven by an electric motor, which is coupled to the primary structure via a spring. Fig. 1 depicts the RPA attached to a primary structure. As the pendulums are turning above a critical speed, they would swing up and down when a periodic force is imposed on the primary structure. If the frequency of the external excitation is close to one of the RPA's natural frequencies, the device will oscillate in such a way as to balance the external force, thereby minimizing the oscillations of the primary structure.

For the purpose of analysis the rotational pendulum is modeled as a lumped mass connected by a massless link, and the primary structure is simplified to be a mass-spring-damper subject to a harmonic force. The dynamic equations governing the overall system depicted in Fig. 1 are derived using Lagrange's equations as follows.

The kinetic energy (denoted by T) and the potential energy (denoted by V) of the system are, respectively,

$$T=\frac{1}{2}m_0[(\ell\dot{\theta}\sin\theta+\dot{x}_1)^2+(\ell\dot{\theta}\cos\theta)^2+(\ell\dot{\phi}\sin\theta)^2]+\frac{1}{2}m_1\dot{x}_1^2+\frac{1}{2}m_2\dot{x}_2^2 \tag{1}$$

$$V=m_0g\ell(1-\cos\theta)+\frac{1}{2}k_1(x_1-x_2)^2+\frac{1}{2}k_2x_2^2 \tag{2}$$

where ℓ is the length of the pendulum arm, m_0 is the lumped mass of the pendulums (each being $m_0/2$), m_1 is the combined mass of the motor and its holder, k_1 is the stiffness of the coupling spring, m_2 is the mass of the primary structure, k_2 is the stiffness of the primary structure, x_1 is the displacement of the RPA, x_2 is the displacement of the primary structure, θ is the vertical angle of the pendulum, and $\dot{\phi}$ is the rotational speed of the pendulums.

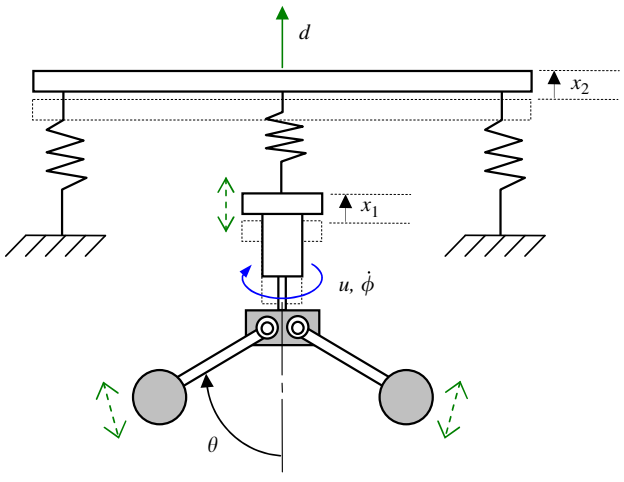

Fig. 1. Schematic of the 2-degree-of-freedom RPA. Each pendulum's arm extends to a certain equilibrium angle with the vertical axis when spinning at a constant speed, and will oscillate vertically if the primary structure is excited by a periodic force.

Let

$$\mathcal{L} = T - V \tag{3}$$

The Lagrange equations for the coordinates of x_2, x_1, θ, and ϕ are, respectively, formulated to be

$$\frac{\mathrm{d}}{\mathrm{d}t}\left(\frac{\partial \mathcal{L}}{\partial \dot{x}_2}\right) - \frac{\partial \mathcal{L}}{\partial x_2} = d - b_2\dot{x}_2 - b_1(\dot{x}_2 - \dot{x}_1) \tag{4}$$

where d is the excitation force to the primary structure, b_2 and b_1 are the damping coefficients associated with, respectively, $\dot{x}_2$ and $\dot{x}_2 - \dot{x}_1$,

$$\frac{\mathrm{d}}{\mathrm{d}t}\left(\frac{\partial \mathcal{L}}{\partial \dot{x}_1}\right) - \frac{\partial \mathcal{L}}{\partial x_1} = -b_1(\dot{x}_1 - \dot{x}_2) \tag{5}$$

$$\frac{\mathrm{d}}{\mathrm{d}t}\left(\frac{\partial \mathcal{L}}{\partial \dot{\theta}}\right) - \frac{\partial \mathcal{L}}{\partial \theta} = -b_0\dot{\theta} \tag{6}$$

where b_0 is the damping coefficient associated with $\dot{\theta}$, and

$$\frac{\mathrm{d}}{\mathrm{d}t}\left(\frac{\partial \mathcal{L}}{\partial \dot{\phi}}\right) - \frac{\partial \mathcal{L}}{\partial \phi} = u - b_R\dot{\phi} \tag{7}$$

where u is the torque applied to the rotor and b_R is the damping coefficient associated with $\dot{\phi}$.

From Eqs. (4) to (7) the dynamic equations can be derived to be

$$m_2\ddot{x}_2 + (k_1 + k_2)x_2 - k_1x_1 + (b_1 + b_2)\dot{x}_2 - b_1\dot{x}_1 = d \tag{8}$$

$$m_0\ell\ddot{\theta}\sin\theta + (m_0 + m_1)\ddot{x}_1 + m_0\ell\dot{\theta}^2\cos\theta + k_1(x_1 - x_2) + b_1(\dot{x}_1 - \dot{x}_2) = 0 \tag{9}$$

$$m_0\ell^2\ddot{\theta} + m_0\ell(\ddot{x}_1 + g)\sin\theta - \frac{1}{2}m_0\ell^2\dot{\phi}^2\sin 2\theta + b_0\dot{\theta} = 0 \tag{10}$$

$$m_0\ell^2(\ddot{\phi}\sin^2\theta + \dot{\phi}\dot{\theta}\sin 2\theta) + b_R\dot{\phi} = u \tag{11}$$

2.1. Dynamics of the RPA

To derive the dynamic equations governing the RPA, the primary structure is held still such that $\ddot{x}_2 = \dot{x}_2 = x_2 = 0$. Eq. (9) is thus reduced to be

$$m_0\ell\ddot{\theta}\sin\theta + (m_0 + m_1)\ddot{x}_1 + m_0\ell\dot{\theta}^2\cos\theta + k_1x_1 + b_1\dot{x}_1 = 0 \tag{12}$$

Eqs. (10)–(12) are the governing equations for the RPA. The two natural modes of vibrations for the RPA are sketched in Fig. 2. Note that for the first mode x_1 and θ are in phase; for the second mode x_1 and θ are 180° out of phase. Before calculation of the natural frequencies, the equilibrium angle for a constant rotational speed must be obtained.

When the pendulums are regulated at a constant speed, ω_0, the equilibrium vertical angle θ_0 can be calculated by setting $\ddot{\theta} = \ddot{x}_1 = \dot{\theta} = 0$ in Eq. (10):

$$m_0\ell g\sin\theta_0 - \frac{1}{2}m_0\ell^2\omega_0^2\sin 2\theta_0 = 0 \tag{13}$$

The equilibrium angle is solved from the previous equation to be

$$\theta_0 = \begin{cases} 0 & \text{if } \omega_0 \le \sqrt{\dfrac{g}{\ell}} \\ \cos^{-1}\dfrac{g}{\ell\omega_0^2} & \text{if } \omega_0 > \sqrt{\dfrac{g}{\ell}} \end{cases} \tag{14}$$

Eq. (14) implies that for the RPA to maintain a nonzero equilibrium angle, it must be turning at a speed larger than the natural frequency of a corresponding simple pendulum.

Denote the deviations about the equilibrium angle θ_0 and the associated constant speed ω_0 to be

$$q = \theta - \theta_0 \tag{15}$$

$$p = \dot{\phi} - \omega_0 \tag{16}$$

Assume the control input u to be

$$u = b_R\omega_0 + k_P(\omega_0 - \dot{\phi}) \tag{17}$$

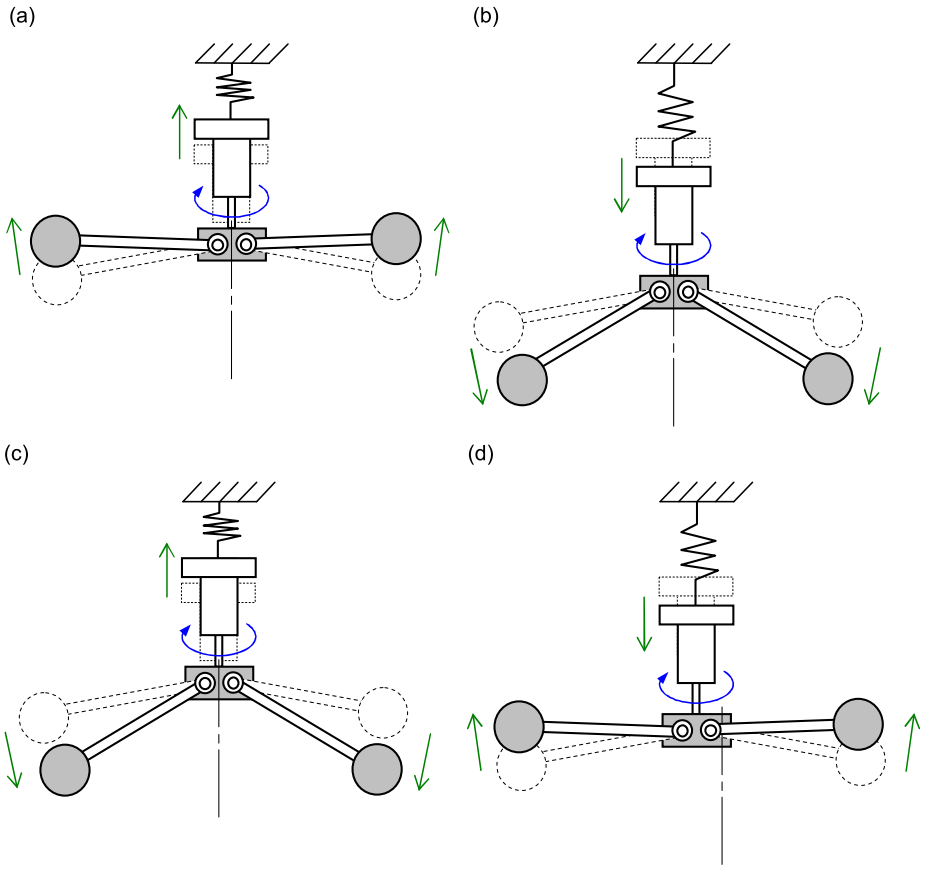

Fig. 2. Two characteristic modes of vibrations: the first mode (a,b) and the second mode (c,d).

where k_P is a positive constant, such that the pendulum is regulated at the speed ω_0. Using Eqs. (14)–(17), the linearized equations for Eqs. (12), (10), and (11) about the speed ω_0 and the corresponding equilibrium angle θ_0 can be derived to be, respectively,

$$(m_0\ell\sin\theta_0)\ddot{q}+(m_0+m_1)\ddot{x}_1+k_1x_1+b_1\dot{x}_1=0 \tag{18}$$

$$m_0\ell^2\ddot{q}+(m_0\ell\sin\theta_0)\ddot{x}_1+m_0\ell^2\omega_0^2\sin^2\theta_0 q-m_0\ell^2\omega_0\sin2\theta_0 p+b_0\dot{q}=0 \tag{19}$$

$$m_0\ell^2\sin^2\theta_0\dot{p}+m_0\ell^2\omega_0\sin2\theta_0\dot{q}+(b_R+k_P)p=0 \tag{20}$$

2.2. Natural frequencies of the RPA

To calculate the natural frequencies for the system of Eqs. (18)–(20), the damping terms must be dropped. Moreover, solutions can be obtained only if either $p=0$ or $b_R+k_P=0$. If $p=0$, Eqs. (18) and (19) are decoupled from Eq. (20); if $b_R+k_P=0$, from Eq. (20) p is negatively proportional to q so that the term associated with p in Eq. (19) can be replaced by q.

We will first examine the situation where the speed perturbation p in Eq. (19) is negligible. This is the case if b_R+k_P in Eq. (20) is large enough: The last term in the left hand side of Eq. (20) dominates if $b_R+ k_P$ is large enough, implying that p tends to zero if b_R+k_P tends to infinity. (This can also be confirmed later by Eq. (22).) In such a case the natural frequencies for vertical vibrations are determined by Eqs. (18) and (19), with the terms associated with damping (b_0, b_1) and p dropped. In matrix form, we have

$$\begin{bmatrix} m_0+m_1 & m_0\ell\sin\theta_0 \\ m_0\ell\sin\theta_0 & m_0\ell^2 \end{bmatrix}\begin{pmatrix}\ddot{x}_1\\ \ddot{q}\end{pmatrix}+\begin{bmatrix} k_1 & 0 \\ 0 & m_0\ell^2\omega_0^2\sin^2\theta_0 \end{bmatrix}\begin{pmatrix}x_1\\ q\end{pmatrix}=\mathbf{0} \tag{21}$$

Eq. (21) indicates that the stiffness matrix of the RPA is dependent on ω_0. The stiffness is thus variable by changing the rotational speed. Physically this can be explained by analogy with the vibration of a simple pendulum (illustrated in Fig. 3). The natural frequency of a simple pendulum is $\sqrt{g/\ell}$, where ℓ is the length and g is the gravitational acceleration. Vibrations of the simple pendulum are on a horizontal plane *perpendicular* to the gravitational force (Fig. 3a). By spinning

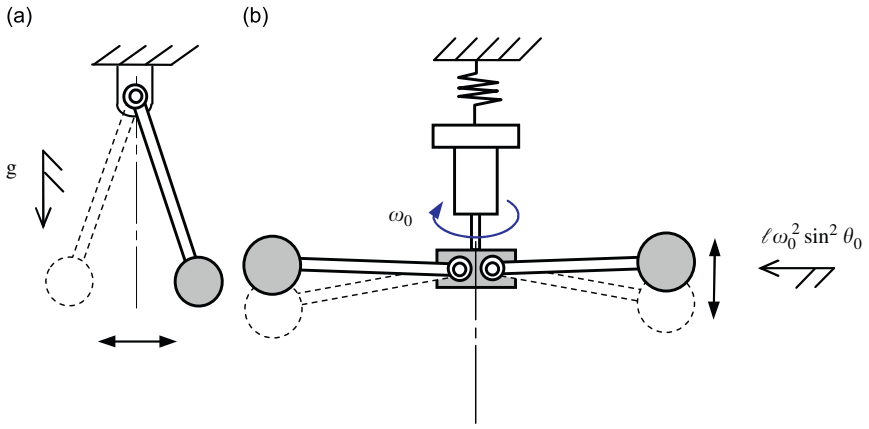

Fig. 3. Analogy between a simple pendulum and the RPA. The vertical gravitational force is replaced by horizontal centrifugal forces.

the pendulum, we effectively change the vertical force field to a near-horizontal centrifugal force field (Fig. 3b), so that vertical vibration of the pendulum is possible. Besides, since the centrifugal acceleration is proportional to the square of the rotational speed, the effective "g" is raised by increasing the speed of rotation. As far as vibrations are concerned, the gravitational force imposing on the simple pendulum is replaced by a centrifugal force of $m_0\ell\omega_0^2\sin^2\theta_0$ on the rotational pendulums.

Next we take the effects of rotational dynamics into account; that is, coupling between p and q is considered. Using Laplace transform, we may express Eq. (20) to be

$$P(s) = -\frac{m_0\ell^2\omega_0 \sin 2\theta_0 s}{m_0\ell^2 \sin^2\theta_0 s + (b_R + k_P)} Q(s) \tag{22}$$

From Eq. (22) it is seen that if k_P is large enough, p is negligible and Eq. (21) holds. Considering the opposite extreme situation where $b_R + k_P = 0$, we have from Eq. (22)

$$P(s) = -\frac{m_0\ell^2\omega_0 \sin 2\theta_0 s}{m_0\ell^2 \sin^2\theta_0 s} Q(s) = -\frac{2\omega_0 \cos\theta_0}{\sin\theta_0} Q(s) \tag{23}$$

Physically the above equation means that, in the absence of external torque, the rotational speed decreases (p negative) as the pendulum link extends (q positive), and the speed increases (p positive) as the link contracts (q negative), in such a way as to keep *rotational momentum* invariant.

Substituting Eq. (23) into Eq. (19) and ignoring the term associated with b_0, we have

$$m_0\ell^2\ddot{q} + (m_0\ell\sin\theta_0)\ddot{x}_1 + m_0\ell^2\omega_0^2(\sin^2\theta_0 + 4\cos^2\theta_0)q = 0 \tag{24}$$

Accordingly the stiffness matrix in Eq. (21) is modified to be

$$\begin{bmatrix} k_1 & 0 \\ 0 & m_0\ell^2\omega_0^2(1+3\cos^2\theta_0) \end{bmatrix} \tag{25}$$

Fig. 4 shows the relations between the equilibrium speed and the characteristic frequencies of the vibration absorber. The parameters used in the calculations are as follows: $m_0 = 0.126$ kg, $m_1 = 0.382$ kg, $k_1 = 1427$ N/m, and $\ell = 87$ mm. They are consistent with the parameters of the experimental setup which will be detailed later. The solid curves are obtained from the mass and stiffness matrices of Eq. (21), while the circles are obtained using the stiffness matrix of Eq. (25). It is seen that the circles match the solid curves except for low rotational speeds, at which the fundamental natural frequency is higher when considering the variations of rotational speeds. This figure indicates that in practice the coupling between p and q can be neglected as far as the natural frequencies for vertical vibration are concerned.

2.3. Time response

To illustrate the performance of the RPA, simulation results on the system of Eqs. (8)–(11) are shown in Fig. 5, where the primary structure is subject to a harmonic excitation with a frequency of 12 Hz (75.4 rad/s). The parameters of the RPA are the same as in the previous subsection, and $m_2 = 1$ kg, $k_2 = 1000$ N/m, $b_2 = 10$ N s/m. From Fig. 4, for the RPA to possess a natural frequency of 75.4 rad/s, the rotational speed should be about 54 rad/s. In the simulation the target speed (ω_0) is initially set at 50 rad/s, then raised to 54 rad/s after 10 s, and raised further to 60 rad/s after 20 s. It is seen from Fig. 5 that when the target speed is right, vibrations of the primary structure are minimized. The performance deteriorates if the RPA

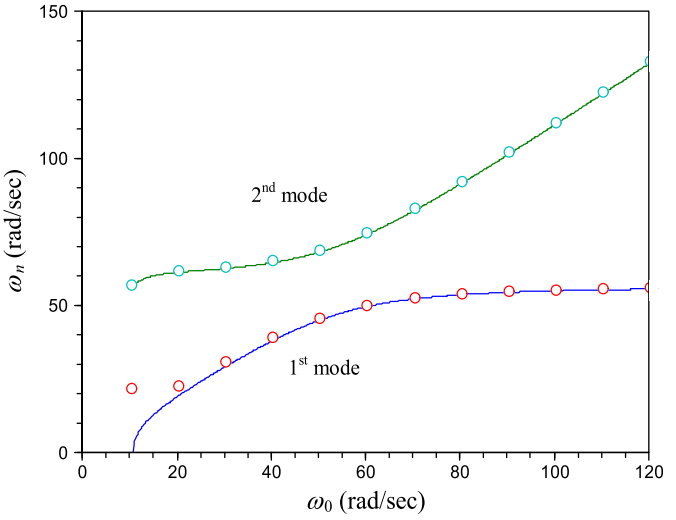

Fig. 4. Calculated characteristic frequencies of the pendulum absorber versus nominal rotational speeds: the solid curves are obtained assuming constant rotational speeds and the circles assuming freely fluctuating speeds (about a nominal, equilibrium value).

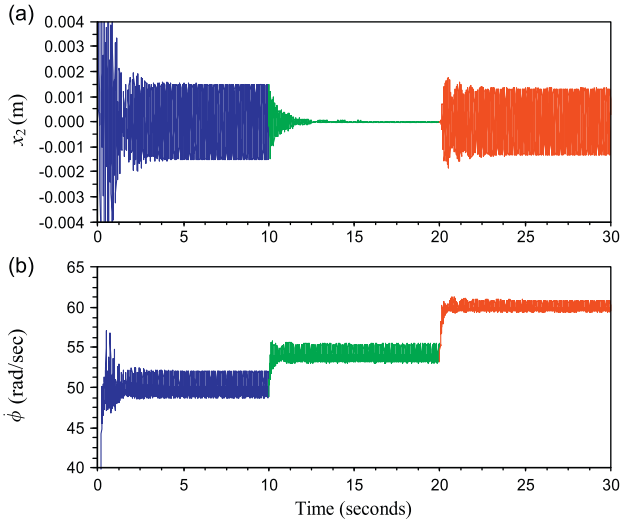

Fig. 5. Time response of the system for various rotational speeds: (a) displacement of the primary structure; (b) rotational speed. The target speed (ω_0) is switched from 50 to 54 rad/s at 10 s, and from 54 to 60 rad/s at 20 s.

is significantly under- or over-driven. Also note that the rotational speed fluctuates about ω_0 due to vertical oscillations of the rotational arm.

3. Tuning of the rotational speed by phase detection

Vibration of the primary structure is minimized if the excitation frequency coincides with one of the natural frequencies of the RPA, as illustrated in Fig. 6. The natural frequencies of the RPA depend on the rotational speed ω_0, which should be adjusted according to the excitation frequency. The speed can be tuned in one of two ways. The first is by table lookup: The natural frequency versus rotational speed (ω_n–ω_0) table is first constructed as in Fig. 4. By measuring the excitation frequency, the operational speed can then be set according to the table. This method is straightforward but subject to modeling uncertainties and parameter variations.

The second method is to measure the phase angle between the displacement of the primary structure (x_2) and the displacement of the RPA (x_1). In practice this can be done by measuring the respective accelerations, namely $\ddot{x}_2$ and $\ddot{x}_1$. From Eq. (9) and referring to Eq. (21), the linearized equation relating x_2 to the variables x_1 and q can be written to be

$$\begin{bmatrix} m_{11} & m_{10} \\ m_{10} & m_{00} \end{bmatrix} \begin{pmatrix} \ddot{x}_1 \\ \ddot{q} \end{pmatrix} + \begin{bmatrix} k_1 & 0 \\ 0 & k_0 \end{bmatrix} \begin{pmatrix} x_1 \\ q \end{pmatrix} = \begin{pmatrix} k_1 x_2 \\ 0 \end{pmatrix} \tag{26}$$

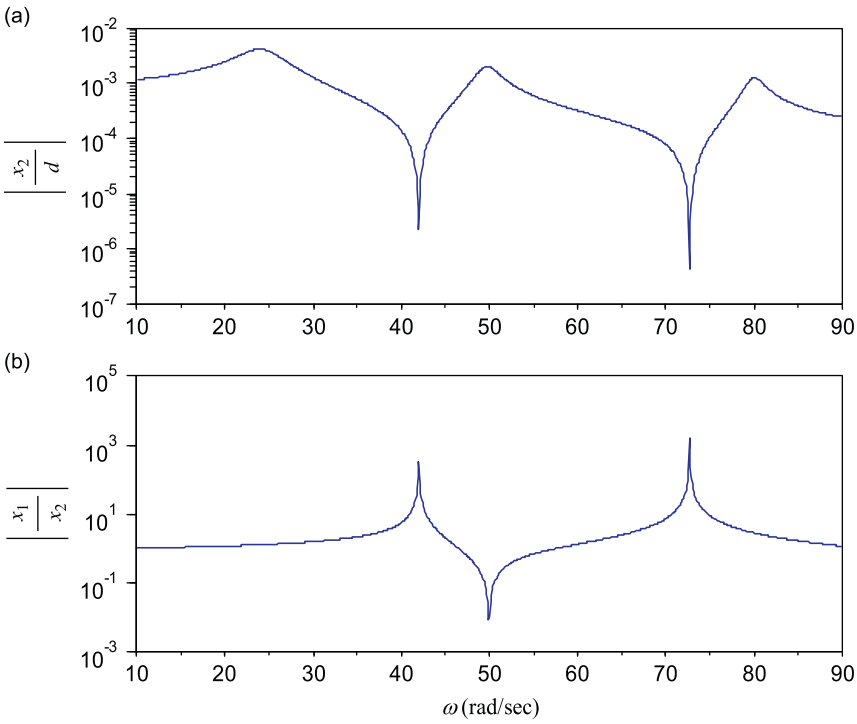

Fig. 6. Frequency response of x_2/d (a) and the response of x_1/x_2 (b). The rotational speed is set to be 50 rad/s. Note that the dips of (a) match the peaks of (b).

where $m_{11}=m_0+m_1$, $m_{10}=m_0\ell\sin\theta_0$, $m_{00}=m_0\ell^2$, $k_0=m_0\ell^2\omega_0^2\sin^2\theta_0$; the damping terms are assumed to be negligible. Let $x_2=e^{i\omega t}$. From Eq. (26) it can be calculated to be

$$\frac{x_1}{k_1x_2}(i\omega)=\frac{-m_{00}\omega^2+k_0}{(m_{11}m_{00}-m_{10}^2)\omega^4-(m_{11}k_0+m_{00}k_1)\omega^2+k_1k_0} \tag{27}$$

$$=\frac{-(\omega^2-\omega_{00}^2)}{(\omega^2-\omega_1^2)(\omega^2-\omega_2^2)} \tag{28}$$

where ω_1 and ω_2 are the first and the second natural frequencies of the RPA, respectively, and $\omega_{00}^2=k_0/m_{00}$. As shown in Fig. 7, the phase between x_2 and x_1 switches from 0° to 180° as the excitation frequency crosses over the first natural frequency, and back to 0 as it crosses over ω_{00} (the zero of the transfer function); the phase switches to 180° again when the excitation frequency crosses over the second natural frequency. This phenomenon can be exploited for the tuning of the natural frequency of the RPA by adjusting the rotational speed. As illustrated in Fig. 8, where the excitation frequency is near the second natural frequency of the RPA, when the RPA is under-driven the phase angle tends toward 0; when over-driven the angle tends toward 180°. Note the difference between Figs. 7 and 8: the former shows the frequency response with a given ω_0, while the latter shows the response for various ω_0's with a given excitation frequency. As will be demonstrated in the next section, the phase angles between x_1 and x_2 can be detected using two accelerometers mounted, respectively, on the RPA and the primary structure.

In this article the target rotational speed (ω_0) is adjusted in an open-loop manner; it is not updated automatically. System stability becomes a critical issue in automatic speed tuning. Generally speaking, to ensure stability the update rate for the target speed must be slower than the fundamental characteristic of the system. However, the issue of closed-loop speed adaptation is beyond the scope of the paper.

4. Experiments

The experimental apparatus is shown in Fig. 9, where the snapshots of operations are also presented showing the pendulums at the states of idling, slowly turning, and fast turning. Parameters of the RPA are measured to be: $m_1=0.382$ kg, $k_1=1427$ N/m, the pendulum link has a length of 100 mm and a weight of 0.023 kg, the pendulum head is a circular disk of diameter 22 mm, height 20 mm, and weight 0.04 kg. The combined mass of the pendulum is therefore 0.063 kg, and the *radius of gyration* is calculated to be 87 mm. In the numerical analysis of the previous sections, m_0 and ℓ are, respectively, assumed to be 0.126 kg (0.63×2) and 87 mm, which is the radius of gyration. (Since a symmetric pair of pendulums is installed, the equivalent mass is doubled.)

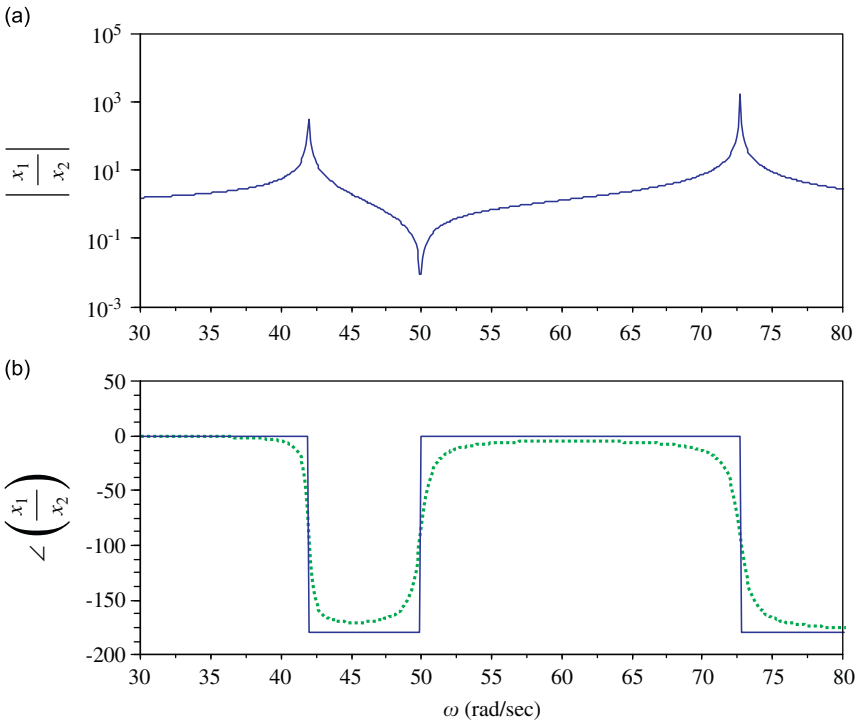

Fig. 7. Frequency response of x_1/x_2 for $\omega_0 = 50$ rad/s: (a) magnitude; (b) phase angle (the solid curve is for the undamped system and the dotted curve is for a lightly damped system.)

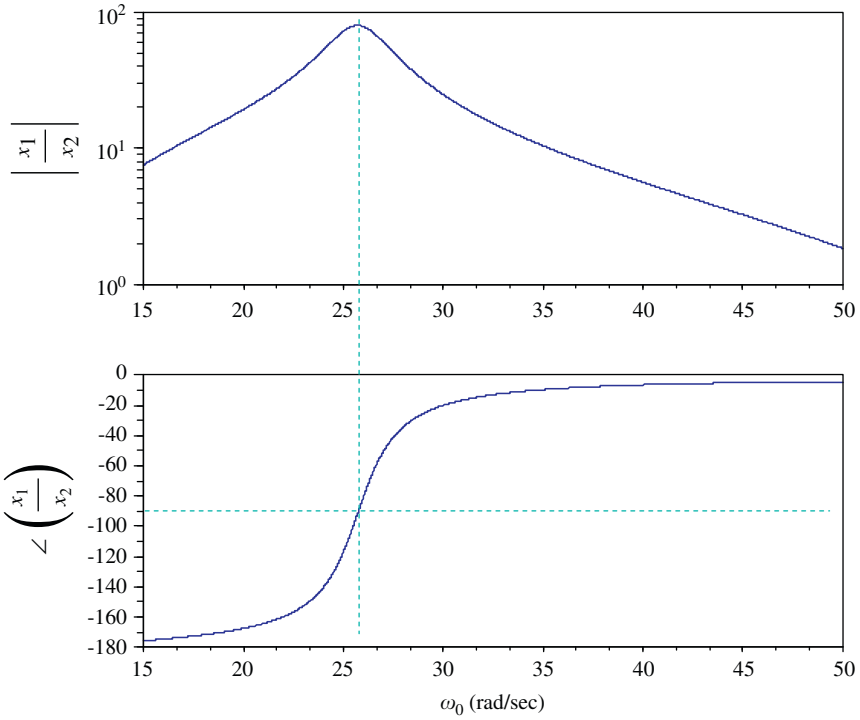

Fig. 8. Magnitudes and phase angles of $x_1/x_2(\omega), \omega = 10$ Hz, for various rotational speeds.

To apply a periodic force to the flexible plate (i.e., the primary structure), a reciprocating pneumatic piston is attached to the plate and is driven by a proportional valve, which is commanded by a function generator. The excitation frequency can thus be set by adjusting the frequency of the signal out of the function generator.

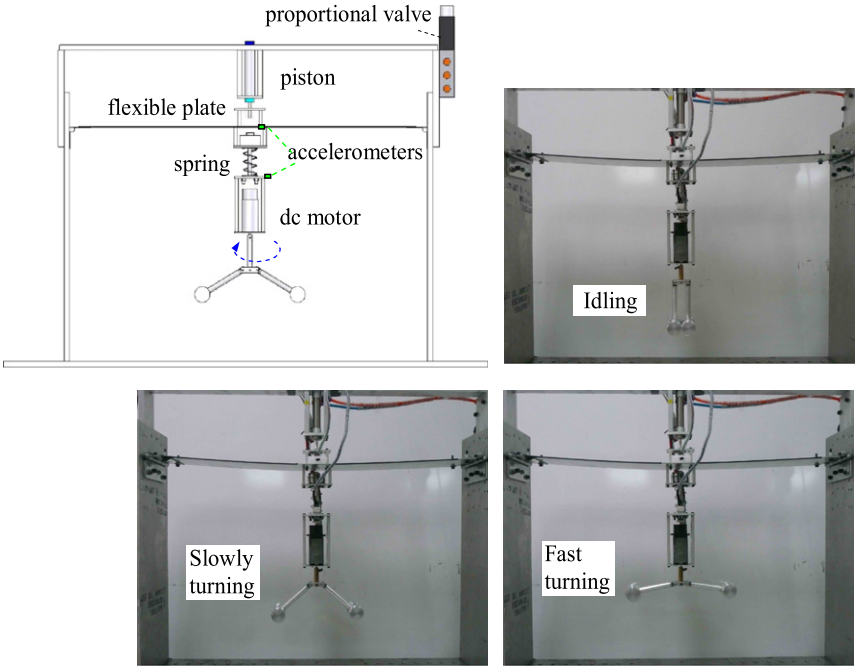

Fig. 9. Experimental apparatus and snapshots of its operation.

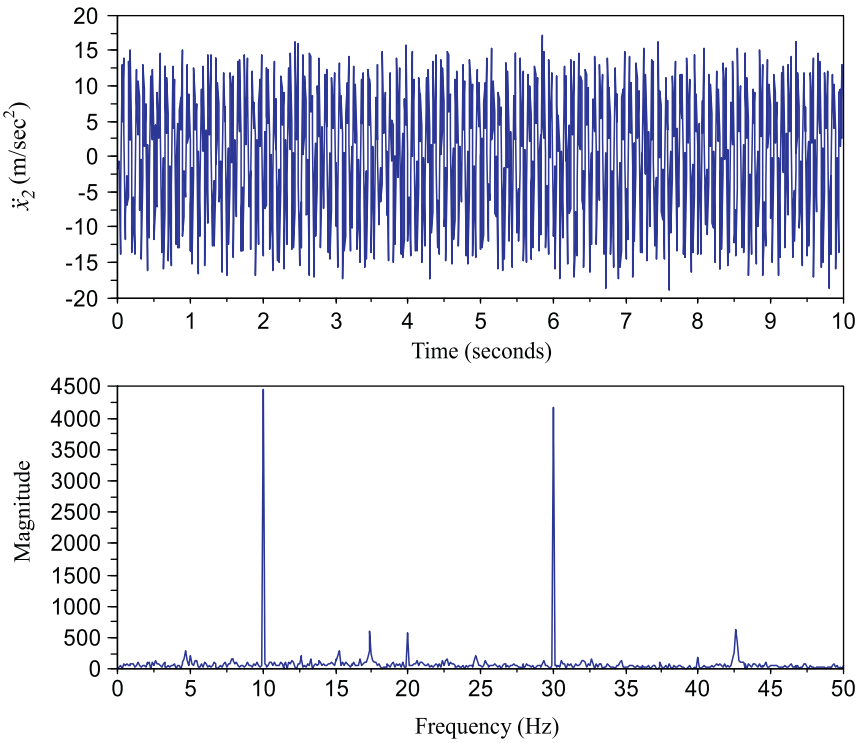

Fig. 10. Acceleration of the flexible plate and its FFT when the RPA is at rest (zero speed).

Figs. 10–12 show the experimental results for an excitation frequency of 10 Hz. The responses of the flexible plate with an idle (uncontrolled) RPA, an optimally tuned RPA, and an over-driven RPA, are compared. Both the time response and the corresponding frequency spectrum by fast Fourier Transform (FFT) are presented. From the uncontrolled response (Fig. 10), it is seen that the excitation contains a 10 Hz component and its overtones, of which the third harmonic is the most

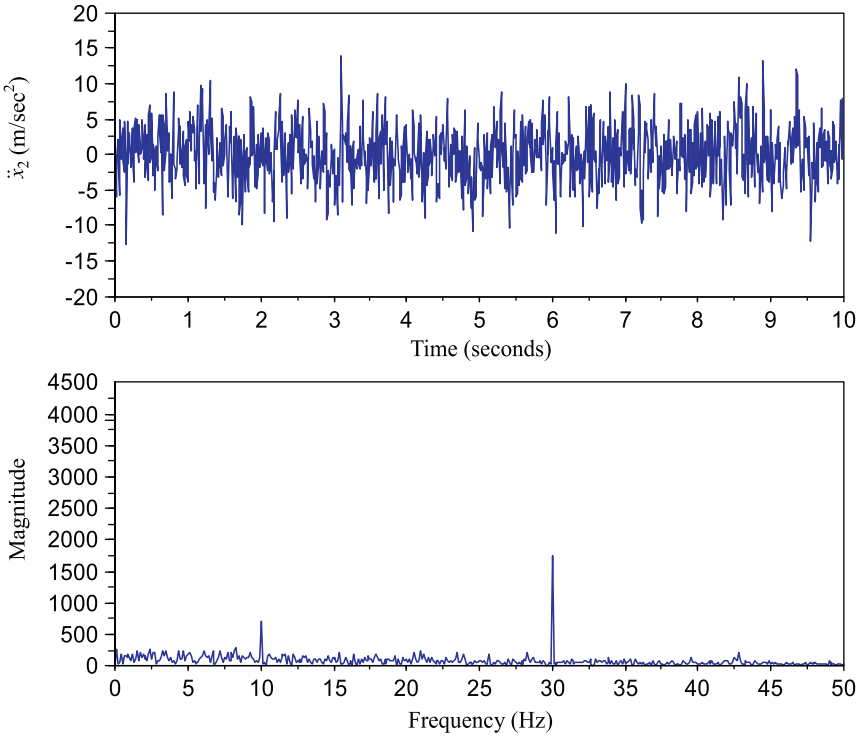

Fig. 11. Acceleration of the flexible plate and its FFT when the rotational speed is set to be 39 rad/s (optimal speed).

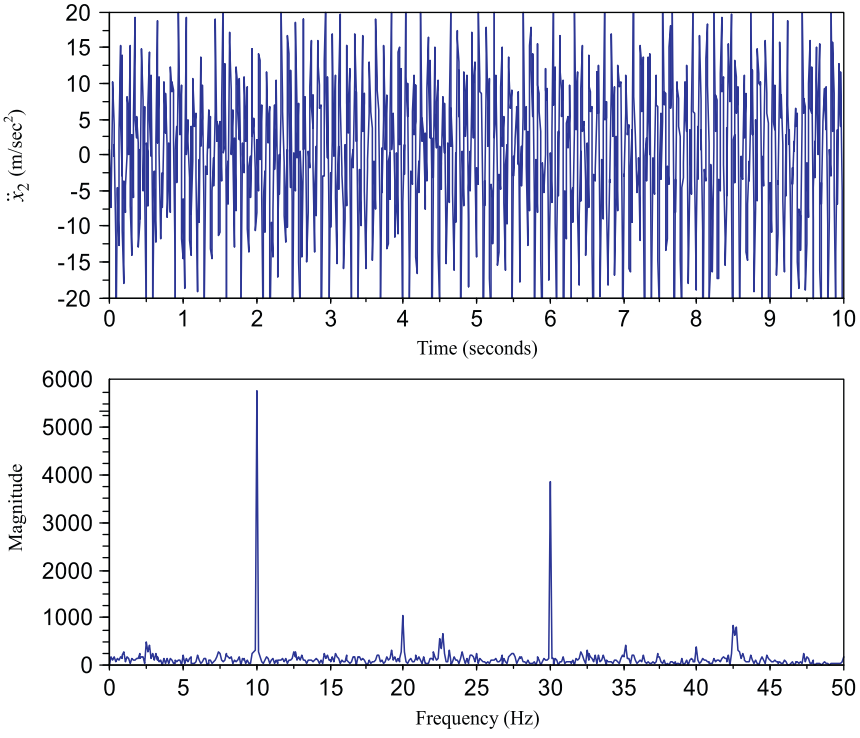

Fig. 12. Acceleration of the flexible plate and its FFT when the rotational speed is set to be 50 rad/s (over-speed).

significant. When the RPA is activated and the rotational speed is set at 6.2 rps (39 rad/s), the vibrations are sharply reduced. From the frequency spectrum it is seen that the fundamental component (10 Hz) is almost cleaned out, while the higher harmonics are also significantly attenuated. The overtones in the measured response can be attributed partly to the

periodic excitation and partly to the nonlinearity of the structure. Since we use a square-wave signal to drive the proportional valve, the input signal contains overtones of the base frequency. In addition, nonlinear dynamics are excited by the pneumatic piston when the displacement is large. That may explain why the overtones are attenuated along with the fundamental frequency.

If the rotational speed is further increased, the characteristic frequency of the RPA deviates from that of the excitation, so that the device is no longer capable of countering the excitation force. It is seen in Fig. 12 that, when the rotational speed is set at 8 rps (50 rad/s), the primary structure vibrates even more severely than the uncontrolled situation.

Table 1 lists the optimal rotational speed corresponding to an excitation frequency varying from 8 to 16 Hz. The optimal speed for a given excitation frequency is found by tuning the speed until the vibration ($\ddot{x}_2$) is minimized. The data are plotted against the analytic results in Fig. 13, where the continuous curves represent calculated values and the plus (+)

Table 1
Optimal rotational speeds for various excitation frequencies.

Excitation frequency (Hz)	8	9	10	11	12	13	14	15	16
(rad/s)	50.3	56.5	62.8	69.1	75.4	81.7	88.0	94.2	100.5
Optimal speed (rad/s)	13.8	30.2	39.0	47.8	54.0	59.1	64.1	71.6	76.7

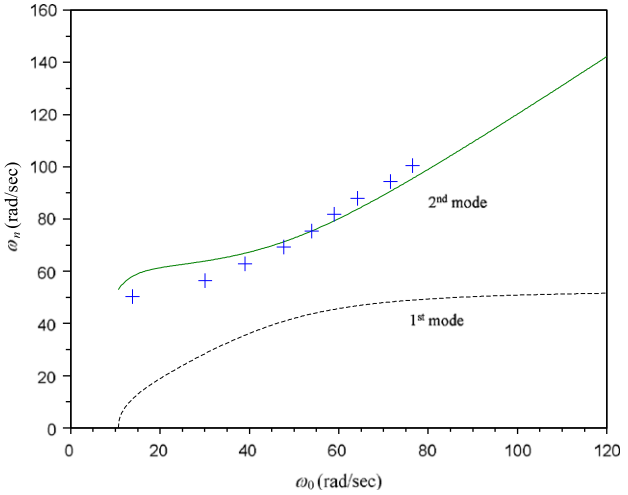

Fig. 13. Measured (+) and calculated characteristic frequencies of the RPA versus rotational speeds. Measured values are from the data on Table 1.

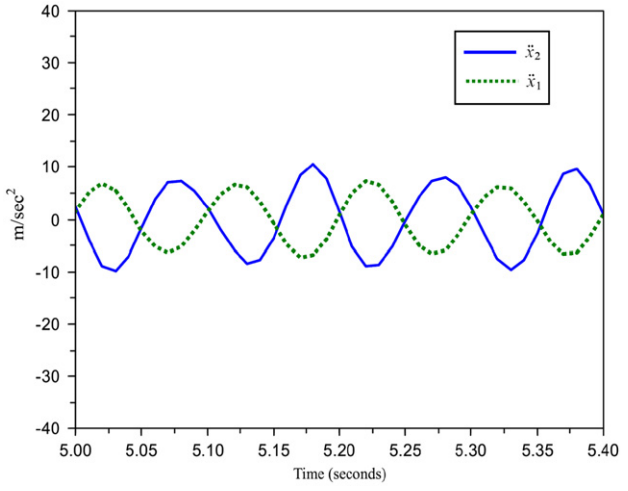

Fig. 14. $\ddot{x}_1$ and $\ddot{x}_2$ are 180° out of phase at zero rotational speed.

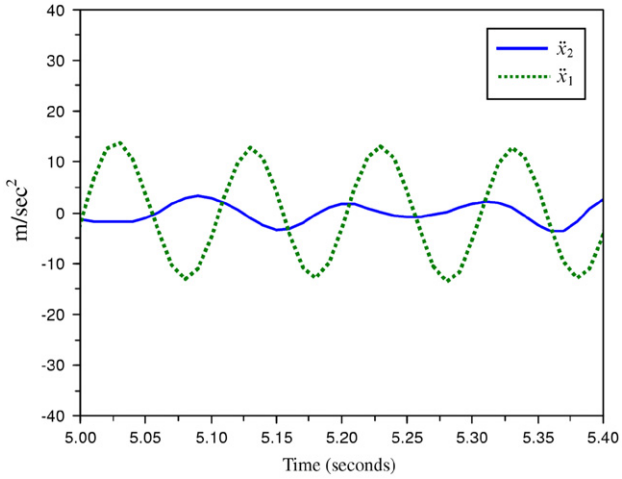

Fig. 15. $\ddot{x}_1$ and $\ddot{x}_2$ are about 90° out of phase at the optimal rotational speed.

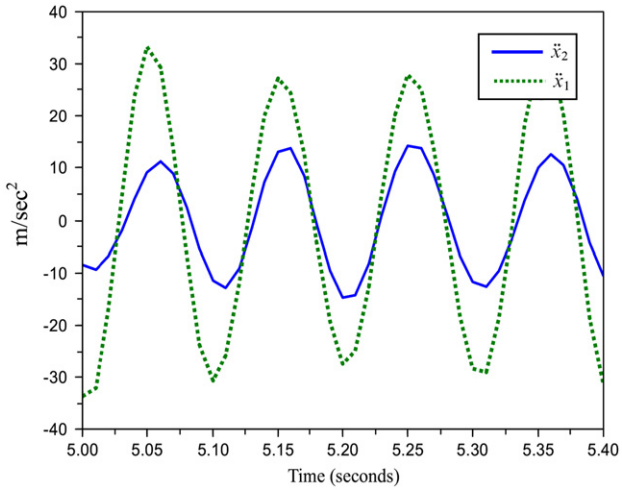

Fig. 16. $\ddot{x}_1$ and $\ddot{x}_2$ are in phase when the pendulums are over-driven at 50 rad/s.

marks are from experiments. It is seen that the experimental data match fairly well with the calculated values (2nd characteristic frequency of the RPA). This confirms the derivation of Section 2.

As mentioned in the previous section, the optimal speed can also be found by observing the phase between $\ddot{x}_2$ and $\ddot{x}_1$. Figs. 14–16 show the phase angles between the filtered accelerations of the primary structure ($\ddot{x}_2$) and the RPA ($\ddot{x}_1$). In these figures the measured acceleration signals are digitally filtered (with a cutoff of 20 Hz) so that the base components are extracted. It is seen (Fig. 14) that the two signals are at opposite phase when the rotational speed is 0. As the turning speed is raised, the phase angle is lowered. It approaches 90° at the optimal rotational speed (Fig. 15). When the pendulums are over-driven, the phase angle drops further toward 0°; the two signals are in phase when the rotational speed is high enough (Fig. 16). The results are consistent with the observations in Section 3.

5. Conclusion

Experimental results on a RPA prototype have shown the effectiveness of the semi-active vibration absorber. The stiffness of the absorber can be dynamically and continuously adjusted by setting the nominal rotational speed. Results of numerical analysis on a simplified model agree well with experimental data as far as natural frequencies are concerned. Exploiting the extra degree of freedom provided by the spring coupler, one may also detect the condition of the absorber via phase estimation and tune the rotational speed accordingly. Further study may include the design of an efficient adaptation algorithm for on-line speed tuning.

References

[1] O. Fischer, Wind-excited vibrations: solution by passive dynamic vibration absorbers of different types, *Journal of Wind Engineering & Industrial Aerodynamics* 95 (2007) 1028–1039.
[2] E. Matta, A. De Stefano, Robust design of mass-uncertain rolling-pendulum TMDs for the seismic protection of buildings, *Mechanical Systems and Signal Processing* 23 (1) (2009) 127–147.
[3] B. Demeulenaere, P. Spaepen, J. De Schutter, Input torque balancing using a cam-based centrifugal pendulum: design procedure and example, *Journal of Sound and Vibration* 283 (1-2) (2005) 1–20.
[4] B.J. Olson, S.W. Shaw, Vibration absorbers for a rotating flexible structure with cyclic symmetry: nonlinear path design, *Nonlinear Dynamics* 60 (1–2) (2010) 149–182.
[5] M.N. Hamouda, G.A. Pierce, Helicopter vibration suppression using simple pendulum absorbers on the rotor blade, *Journal of the American Helicopter Society* 29 (3) (1984) 19–29.
[6] I. Nagasaka, Y. Ishida, T. Koyama, N. Fujimatsu, Vibration suppression of a helicopter fuselage by pendulum absorbers: rigid-body blades with aerodynamic excitation force, *Journal of System Design and Dynamics* 2 (6) (2008) 1230–1238.
[7] O. Cuvalci, A. Ertas, Pendulum as vibration absorber for flexible structures: experiments and theory, *Journal of Vibration and Acoustics* 118 (4) (1996) 558–566.
[8] A. Vyas, A.K. Bajaj, Dynamics of autoparametric vibration absorbers using multiple pendulums, *Journal of Sound and Vibration* 246 (1) (2001) 115–135.
[9] Y. Song, H. Sato, Y. Iwata, T. Komatsuzaki, The response of a dynamic vibration absorber system with a parametrically excited pendulum, *Journal of Sound and Vibration* 259 (4) (2003) 747–759.
[10] S.-T. Wu, Active pendulum vibration absorbers with a spinning support, *Journal of Sound and Vibration* 323 (2009) 1–16.
[11] S.-T. Wu, Y.-Y. Chiu, Y.-C. Yeh, Hybrid vibration absorber with virtual passive devices, *Journal of Sound and Vibration* 299 (1–2) (2007) 247–260.
[12] S.-T. Wu, Y.-J. Shao, Adaptive vibration control using a virtual-vibration-absorber controller, *Journal of Sound and Vibration* 305 (4–5) (2007) 891–903.
[13] S.-T. Wu, J.-Y. Chen, Y.-C. Yeh, Y.-Y. Chiu, An active vibration absorber for a flexible plate boundary-controlled by a linear motor, *Journal of Sound and Vibration* 300 (1–2) (2007) 250–264.
[14] Y. Zhang, A. Alleyne, A simple novel approach to active vibration isolation with electrohydraulic actuation, *Journal of Dynamic Systems, Measurement, and Control* 125 (2003) 125–128.
[15] P. Bonello, M.J. Brennan, S.J. Elliott, Vibration control using an adaptive tuned vibration absorber with a variable curvature stiffness element, *Smart Materials & Structures* 14 (2005) 1055–1065.
[16] K.A. Williams, G.T.-C. Chiu, R.J. Bernhard, Nonlinear control of a shape memory alloy adaptive tuned vibration absorber, *Journal of Sound and Vibration* 288 (2005) 1131–1155.
[17] E. Rustighi, M.J. Brennan, B.R. Mace, Real-time control of a shape memory alloy adaptive tuned vibration absorber, *Smart Materials & Structures* 14 (2005) 1184–1195.
[18] C. Hirunyapruk, M.J. Brennan, B.R. Mace, W.H. Li, A tunable magneto-rheological fluid-filled beam-like vibration absorber, *Smart Materials & Structures* 19 (5) (2010).
[19] J. Liu, K. Liu, A tunable electromagnetic vibration absorber: characterization and application, *Journal of Sound and Vibration* 295 (2006) 708–724.
[20] R.I. Wright, M.R.F. Kidner, Vibration absorbers: a review of applications in interior noise control of propeller aircraft, *Journal of Vibration and Control* 10 (2004) 1221–1237.